ISSN 0006-2979, Biochemistry (Moscow), 2008, Vol. 73, No. 10, pp. 1063-1075. © Pleiades Publishing, Ltd., 2008.
Original Russian Text © I. V. Kuvykin, A. V. Vershubskii, V. V. Ptushenko, A. N. Tikhonov, 2008, published in Biokhimiya, 2008, Vol. 73, No. 10, pp. 1329-1343.
Originally published in Biochemistry (Moscow) On-Line Papers in Press, as Manuscript BM08-016, September 14, 2008.

Oxygen as an Alternative Electron Acceptor in the Photosynthetic Electron Transport Chain of C_3 Plants

I. V. Kuvykin, A. V. Vershubskii, V. V. Ptushenko, and A. N. Tikhonov*

Faculty of Physics, Lomonosov Moscow State University, 119992 Moscow, Russia; E-mail: an_tikhonov@mail.ru

Received January 18, 2008
Revision received May 6, 2008

Abstract—This study deals with effects of oxygen on the kinetics of P_{700} photoinduced redox transitions and on induction transients of chlorophyll fluorescence in leaves of C_3 plants *Hibiscus rosa-sinensis* and *Vicia faba*. It is shown that the removal of oxygen from the leaf environment has a conspicuous effect on photosynthetic electron transport. Under anaerobic conditions, the concentration of oxidized P_{700} centers in continuous white light was substantially lower than under aerobic conditions. The deficiency of oxygen released non-photochemical quenching of chlorophyll fluorescence, thus indicating a decrease in the trans-thylakoid pH gradient (ΔpH). Quantitative analysis of experimental data within the framework of an original mathematical model has shown that the steady-state electron flux toward oxygen in Chinese hibiscus leaves makes up to ~40% of the total electron flow passing through photosystem 1 (PS1). The decrease in P^+_{700} content under anaerobic conditions can be due to two causes: i) the retardation of electron outflow from PS1, and ii) the release of photosynthetic control (acceleration of electron flow from PS2 to P^+_{700}) owing to lower acidification of the intra-thylakoid space. At the same time, cyclic electron transport around PS1 was not stimulated in the oxygen-free medium, although such stimulation seemed likely in view of possible rearrangement of electron flows on the acceptor side of PS1. This conclusion stems from observations that the rates of P^+_{700} reduction in DCMU-poisoned samples, both under aerobic and anaerobic conditions, were negligibly small compared to rates of electron flow from PS2 toward P^+_{700} in untreated samples.

DOI: 10.1134/S0006297908100027

Key words: C_3 plants, chloroplasts, electron transport, EPR, non-photochemical fluorescence quenching, mathematical modeling

Investigation of alternative pathways of photosynthetic electron transport is a challenging problem in biochemistry and biophysics of photosynthesis. In oxygenic photosynthetic systems, cyclic electron flow around photosystem 1 (PS1) is known to operate in addition to the main noncyclic pathway transporting electrons from water to $NADP^+$ [1-10]. When molecular oxygen rather than $NADP^+$ acts as a terminal electron acceptor in PS1, it is eventually reduced to water during operation of pseudocyclic electron transport (water–water cycle: $H_2O \rightarrow PS2 \rightarrow PS1 \rightarrow O_2 \rightarrow H_2O$) [11-16]. The existence of various electron transport pathways optimizes the operation of the photosynthetic apparatus (see reviews [17-20]). Although electron flows through cyclic and pseudocyclic chains do not reduce $NADP^+$, they generate the transmembrane electrochemical gradient for protons needed for operation of the ATP synthase complexes. Thus, the stoichiometric ATP/NADPH ratio of 3 : 2 required for functioning of the Calvin cycle is attained.

Data concerning the functional role of alternative electron transport pathways are controversial (see reviews [1, 2, 7, 12-15] and references therein). In particular, the physiological role of oxygen as an alternative electron acceptor in PS1 (the Mehler reaction) of C_3 plants *in vivo* remains a matter of discussion. According to some reports, pseudocyclic electron transport is of minor importance and contributes about 10% of total electron flow between PS2 and PS1 [13-15, 21]. Therefore, many authors suppose that the Mehler reaction has no principal role in the functioning of the photosynthetic machinery in plants [13-15, 21]. However, there is another view on the role of oxygen in plant metabolism. It was shown, for example, that oxygen is needed for activation of Rubisco [22]. Furthermore, there is experimental evidence that

Abbreviations: DCMU) 3-(3,4-dichlorophenyl)-1,1-dimethylurea (diuron); EPR) electron paramagnetic resonance; Fd) ferredoxin; NDH) NAD(P)H-dehydrogenase; PAM) pulse amplitude modulated (fluorometry); PS1 and PS2) photosystems 1 and 2; Q and QH_2) oxidized and reduced plastoquinone forms, respectively.

* To whom correspondence should be addressed.

pseudocyclic electron transport (the water–water cycle) can serve as a starter system initiating energy-dependent events of photosynthesis in chloroplasts during early stages of illumination [13, 23-25]. It is supposed that the electron efflux from PS1 to oxygen prevents excessive accumulation of reduced electron carriers on the acceptor side of PS1 [12-14, 16, 25-27]. According to various estimates (see reviews [2, 19, 20]), the required ATP/NADPH ratio can be achieved if the electron flux diverted to oxygen and the cyclic electron transport chain constitutes a minor fraction, even as small as 10-15% of the noncyclic electron flow to $NADP^+$. The relative contribution of pseudocyclic electron transport may vary depending on physiological factors. For example, the electron flows related to CO_2 and O_2 reduction in C_3 plants are redistributed upon lowering of leaf water content [7, 9, 28].

Regulatory photosynthetic events in intact systems with oxygenic photosynthesis are reflected by multiphase kinetics of P_{700} redox transitions observed in leaves [29-31], algae [32], and cyanobacteria [33, 34]. The complex kinetics of P_{700} photooxidation is determined by various processes affecting the ratio of electron influx and efflux in PS1. Several such processes can be listed: activation of the Calvin cycle enzymes [35] resulting in accelerated electron efflux from PS1; rearrangement of electron flows through different pathways (cyclic/noncyclic electron transport) [1-10]; redistribution of mobile light-harvesting complexes between PS2 and PS1 ("state 1" ↔ "state 2" transitions) [36]; retardation of electron transport at the chain segment between PS2 and PS1 (photosynthetic control phenomenon) [37-42]; and energy dissipation in light-harvesting antenna of PS2 [43-48]. The latter two processes are related to photoinduced acidification of the thylakoid lumen.

The aim of this study was to assess proportions of photosynthetic electron flows passing through PS1 in the *in situ* chloroplasts of C_3 plants and to examine the influence of external factors on these flows. With this in mind, we studied effects of illumination prehistory and atmospheric composition (O_2, CO_2) on light-induced P_{700} redox transients and chlorophyll fluorescence induction curves in leaves of *Hibiscus rosa-sinensis* and *Vicia faba*. An original mathematical model of light stages in photosynthesis was employed for the analysis of the experimental data.

MATERIALS AND METHODS

Materials. The main materials were leaves of a mature Chinese hibiscus plant (*Hibiscus rosa-sinensis*) and leaves of 2- to 3-week-old bean seedlings (*Vicia faba*, cv. Russkie chernye). For measurements of EPR spectra, the leaf segments (3 × 30 mm) were cut out and fixed in a transparent plastic holder; the holder design ensured free access of atmospheric oxygen and other gases to the leaf sample. The holder with a sample was placed into a quartz tube positioned in the middle of a rectangular resonator of the EPR spectrometer. Chlorophyll fluorescence was measured with a portable fluorometer using freshly excised leaf segments (10 × 10 mm, measurements *in situ*) or whole leaves of intact plants (measurements *in vivo*). A portable FluorPen fluorometer (FP100; Proton System Instruments, Czechia) with an attached leaf sample was placed into a special housing where the gas composition was controlled.

DCMU (3-(3,4-dichlorophenyl)-1,1-dimethylurea), a PS2 inhibitor, was introduced into leaves by means of vacuum infiltration. To this end, the leaf segment was placed into a 10-ml syringe filled with a 0.1 mM DCMU solution in water–ethanol mixture; the ethanol content never exceeded 2% (v/v). The syringe piston was then rapidly drawn back to create negative pressure that infiltrated the leaf. The control samples were infiltrated with 2% ethanol dissolved in water.

Control of gas composition. During EPR measurements, the sample fixed in the cavity of the EPR spectrometer was inside the quartz tube where the gas composition was controlled by pumping a gas stream containing oxygen, carbon dioxide, and neutral gas (argon or nitrogen) in various proportions. During fluorescence measurements, the sample attached to the fluorometer was placed into a gas-impermeable housing where the gas composition was kept constant. The gas streams passing through the cavity of the EPR spectrometer and through the fluorometer housing were finely adjusted by flow-control valves inserted in the flow path between the gas tanks and the measuring equipment. Concentrations of O_2 and CO_2 in the chamber were monitored by means of Klever-V (Delta Pro, Russia) and C2000 (Oldham, France) gas analyzers.

EPR measurements of P_{700} redox conversions. EPR spectra were measured with a Varian E-4 X-band spectrometer (USA). The EPR spectra attributed to oxidized P^+_{700} reaction centers were recorded at microwave power 10 mW and amplitude of high-frequency (HF) modulation 4 G. To detect redox transients of P_{700}, the magnetic field was fixed on the low-field extremum of the EPR signal assigned to P^+_{700}. The time constant of the instrument was 0.3 sec.

Samples placed in the cavity of the EPR spectrometer were illuminated with white light from a 100 W incandescent tungsten lamp. The light beam was directed to the sample through the transparent window of the resonator. Infrared radiation was cut off with a 5-cm thick water filter. Actinic light intensity at the sample surface was 320 W/m^2.

To standardize the experimental conditions, the sample placed into the EPR spectrometer cavity was first illuminated with white light for 1 min and then adapted to darkness for 10 min. Following this pretreatment, the kinetics of light-induced signal was recorded. According

to a second experimental protocol, the sample was adapted to darkness without pre-illumination.

Measurements of chlorophyll fluorescence in leaves. Chlorophyll fluorescence in leaves was measured with a FluorPen FP100 portable pulse-amplitude-modulated (PAM) fluorometer. This instrument is devised for measurements of fast fluorescence transients (*O-J-I-P*), as well as for determination of non-photochemical fluorescence quenching according to the commonly accepted illumination protocol. Fluorescence was excited by a visible light band peaking at 475 nm (half bandwidth 25 nm). The photon flux density for saturating light pulses was about 3000 $\mu E \cdot m^{-2} \cdot sec^{-1}$ (760 W/m^2); the fluence rate of actinic light was 1500 $\mu E \cdot m^{-2} \cdot sec^{-1}$ (380 W/m^2). When the kinetics of non-photochemical fluorescence quenching was measured, the probing light pulses were applied at a rate of 1 sec^{-1}; the intensity for these pulses was 900 $\mu E \cdot m^{-2} \cdot sec^{-1}$ (230 W/m^2). Fast fluorescence transients induced by actinic light were recorded at sampling intervals varying from 10 μsec to 10 msec.

RESULTS AND DISCUSSION

General features of light-induced P_{700} photooxidation: dependence on illumination prehistory. Electron transport and other metabolic processes depend on illumination prehistory, which is due to regulation of photosynthetic processes [35, 49]. Electron paramagnetic resonance (EPR) is a convenient means to study induction phenomena in optically dense specimens, higher plant leaves in particular. This method is readily suitable for monitoring the state of PS1 reaction centers. Figure 1a shows EPR spectra of Chinese hibiscus leaves placed in darkness (curve *1*) and in light (curve *2*). The light-induced EPR signal has a width of ΔH_{pp} = 8 G (EPR signal I). This signal is attributed to ion-radical P^+_{700}, the oxidized primary electron donor of PS1 [50].

Figure 1b shows representative light-induced changes in EPR signal I in a leaf sample that was dark-adapted after pre-illumination with white light. Left curve was obtained after 10-min dark adaptation, and right curve was measured after short-term (30 sec) dark adaptation. It is seen that the kinetics of P_{700} photooxidation after 10-min dark adaptation is clearly multiphasic. An initial comparatively small (10-20%) jump of the EPR signal I (stage *A*) was followed by a short lag phase and subsequent S-shaped signal increase (stage *B*). The third distinct stage (stage *C*) was manifested as a comparatively slow ($\tau_{1/2}$ ~ 30-60 sec) increase in EPR signal I. After switching off the light, the EPR signal returned to its initial level. Repeated illumination after a short dark

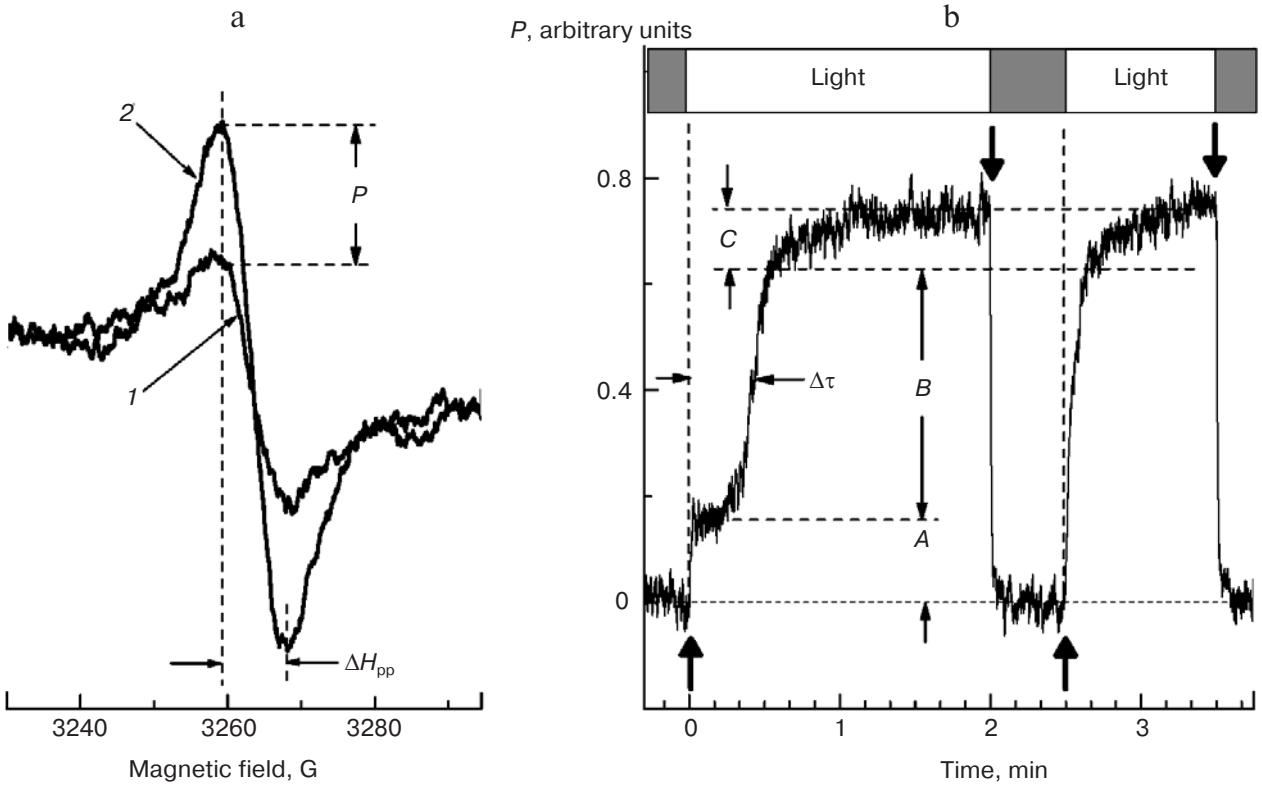

Fig. 1. a) EPR spectra measured on Chinese hibiscus leaves in dark (*1*) and in light (*2*). b) Kinetics of light-induced changes in EPR signal attributed to P^+_{700} in Chinese hibiscus leaves. The plant sample was dark-adapted for 10 min in darkness after 1-min pre-illumination with white light.

period (30 sec) resulted in faster oxidation of P_{700} (Fig. 1b). In this case, the separation between stages *A* and *B* disappeared, and there was no lag phase observed in leaves after long (≥5-10 min) dark adaptation.

The duration of the lag phase preceding the stage *B* signal rise depended on illumination prehistory. Figure 2 displays kinetic curves obtained for two different illumination protocols. In the first case (curve *1*), the freshly prepared leaf sample was adapted to darkness for 10 min without pre-illumination. In the second case (curve *2*), the sample was pre-illuminated with white light for 2 min prior to 10-min dark adaptation. The kinetics of P_{700} oxidation showed clear differences in these two cases. In the leaf adapted to darkness without pre-illumination (curve *1*), the lag phase was longer than in the leaf adapted to darkness after pre-illumination (curve *2*). For all subsequent illumination cycles separated with 10-min dark intervals, the kinetic curves were nearly identical (data not shown). The results indicate that the leaf "memory" of pre-illumination is retained after dark adaptation periods as long as 10 min.

The distinctions in kinetic behavior of EPR signal I in dark-adapted and pre-illuminated leaves might be caused by a series of adaptive changes in the photosynthetic apparatus in response to variable illumination conditions [35]. For example, the Calvin cycle metabolites might be present in larger amounts in pre-illuminated samples (these metabolites can persist for long periods in darkness), which would promote a faster activation of this cycle. The discussion of this topic goes beyond the scope of the present article. We only emphasize that such effects should be taken into account for correct standardization of experimental conditions in studies with intact photosynthetic systems.

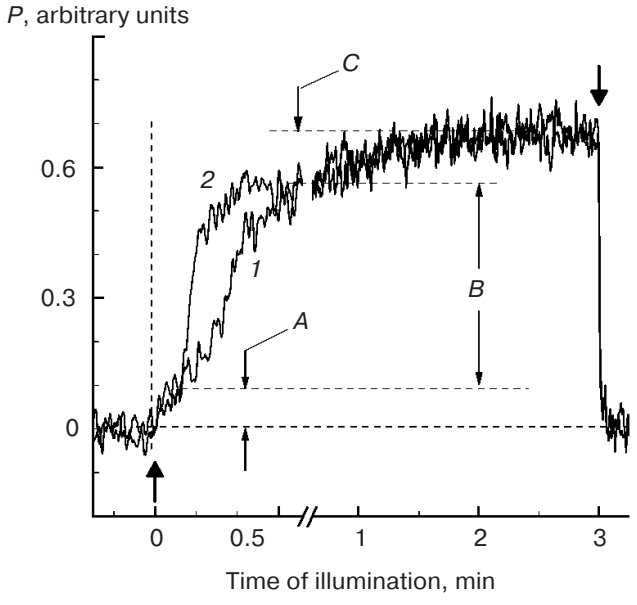

Fig. 2. Kinetics of light-induced changes in EPR signal attributed to P_{700}^+ in Chinese hibiscus leaves: *1*) sample adapted to darkness for 10 min without pre-illumination; *2*) sample adapted to darkness for 10 min after 1-min pre-illumination.

Effect of oxygen on kinetics of light-induced redox conversions of P_{700}. In Fig. 3 redox transients of P_{700} in Chinese hibiscus leaves are compared for aerobic (curve *1*) and anaerobic (curve *2*) conditions. It is seen that the EPR signal I in deaerated samples ($[O_2] < 0.5\%$) increased only slightly upon illumination; the extent of this increase was comparable to the first phase of P_{700} oxidation observed under aerobic conditions ($[O_2] = 21\%$). No further rise of the signal was observed. The strong depression of steady-state concentration of P_{700}^+ under anaerobic conditions can be explained by considering oxygen as an electron acceptor in PS1: the lack of oxygen in this case would result in accumulation of reduced electron carriers on the acceptor side of PS1 [16, 30, 51, 52]. This "over-reduction" of PS1 acceptors should prevent P_{700} photooxidation. It has to be noted that the strong decrease in P_{700}^+ level under anaerobic conditions was mainly due to the removal of oxygen rather than to depletion of endogenous CO_2, a terminal physiological electron acceptor. Although CO_2 content could be depleted, at least partly, during flushing the leaf by inert gas (Ar or N_2), a similar low level of P_{700}^+ was observed during flushing the leaf with oxygen-free gas mixtures ($N_2 + CO_2$ or $Ar + CO_2$) enriched in CO_2 (~0.5-1%) (see further details below, Fig. 8a). This observation proves that the decrease in P_{700}^+ level under anaerobic conditions results basically from the removal of O_2 rather than from possible depletion of endogenous CO_2.

The steady-state concentration of P_{700}^+ is determined not only by the rate of electron outflow from PS1 but also by the rate of electron supply to P_{700}^+. Therefore, it is reasonable to suppose that the decrease in P_{700}^+ level under anaerobic conditions is based on both the retardation of electron outflow from PS1 and acceleration of electron flow toward PS1. The acceleration of electron transport on the PS1 donor side might be caused by various factors, e.g. by the decrease in ΔpH and/or by stimulation of cyclic electron flow around PS1. Cyclic electron transport around PS1 involves both a "short" chain (PS1 → Fd → Q) and a "long" electron transport pathway (PS1 → Fd → NADP → NDH → Q) [1-4]. In addition, endogenous photosynthates (e.g. sugars) and reduced common metabolites exchanged between chloroplasts and mitochondria can also provide electron donors for P_{700}^+. Arnon et al. [53] were among the first to obtain evidence for activation of cyclic photophosphorylation under anaerobic conditions. However, the question of the role of oxygen in regulating electron flows on the acceptor side of PS1 remains a matter of controversy (see reviews [12-15]). Some observations suggest that the removal of oxygen inhibits, rather than stimulates, cyclic electron transport [54].

To assess the contribution of cyclic electron transport and endogenous donors to the total electron flux

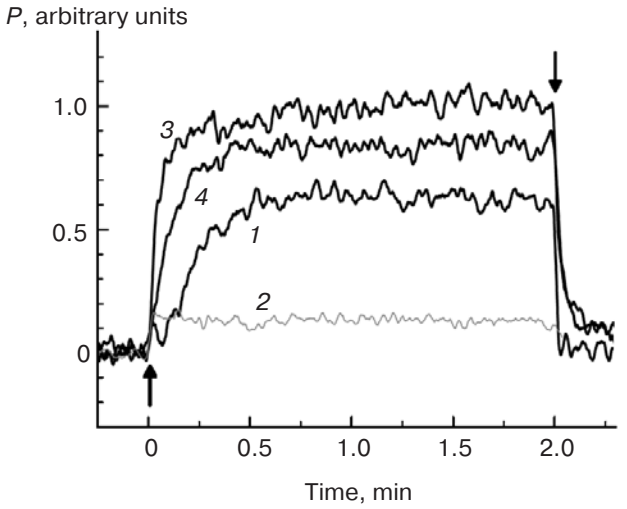

Fig. 3. Light-induced changes of P^+_{700} EPR signal in Chinese hibiscus leaves adapted to darkness (10 min) after pre-illumination with white light (1 min). Adaptation conditions: *1*) control sample under aerobic conditions ($[O_2] = 21\%$); *2*) control sample under anaerobic conditions ($[O_2] < 0.5\%$); *3*) aerobic conditions ($[O_2] = 21\%$), leaf infiltrated with 0.1 mM DCMU; *4*) anaerobic conditions ($[O_2] < 0.5\%$), leaf infiltrated with 0.1 mM DCMU.

arriving to P^+_{700}, we infiltrated Chinese hibiscus leaves with 0.1 mM DCMU solution, since DCMU at this concentration almost completely inhibits PS2 activity. It is seen in Fig. 3 that P_{700} photooxidation proceeded rather fast in the presence of DCMU. The lag phase and P_{700} slow oxidation stage characteristic of untreated leaves were lacking, while the steady-state concentration of P^+_{700} was substantially higher in DCMU-treated than in untreated (control) samples (cf. curves *1* and *3*). In the DCMU-treated leaf, the dark reduction of P^+_{700} takes much longer time ($\tau_{1/2}$ ~ 0.7-0.9 sec) than in untreated samples ($\tau_{1/2}$ < 100 msec). Thus, the contribution of cyclic electron flow to P^+_{700} reduction is substantially smaller than contribution of PS2, which is consistent with the reports that cyclic electron transport in C_3 plants under steady-state conditions constitutes about 10% of linear electron flow [1, 7].

In DCMU-treated leaf samples, like in untreated samples, the kinetics of P_{700} photooxidation was sensitive to oxygen concentration. It is seen in Fig. 3 that P_{700} photooxidation was decelerated after the removal of oxygen (cf. curves *3* and *4*). This effect could be interpreted in a way that the lack of oxygen, capable of draining electrons from PS1, promotes cyclic electron flow around PS1, thus lowering the P^+_{700} content. However, our experiments revealed that the dark reduction of P^+_{700} was not accelerated in the O_2-free environment. The data present evidence that electron supply to P^+_{700} from endogenous donors and cyclic pathway remains slow under anaerobic conditions. It should be noted that, in leaves treated with DCMU, the steady-state content of P^+_{700} under anaerobic conditions was significantly higher (Fig. 3, curve *4*) than in deaerated leaves in the absence of DCMU (Fig. 3, curve *2*). This fact also implies that the electron flux to P^+_{700} in DCMU-treated leaves constitutes a minor portion with respect to electron flux from PS2 in untreated leaves. Thus, we conclude that the retardation of P_{700} photooxidation in DCMU-treated leaves transferred to anaerobic conditions (Fig. 3, curve *4*) cannot result from enhanced electron input to P^+_{700} from cyclic electron transport (and/or from endogenous electron donors).

Effect of oxygen on fast stages in the induction curve of chlorophyll fluorescence. Analysis of fluorescence induction curves provides information on the redox state of the electron transport chain. The dependence of the fluorescence induction curve on illumination prehistory is well characterized; the contribution of various electron transport stages to the shape of the induction curve is also known (see reviews [44, 45, 48, 55]). The influence of illumination prehistory on the kinetics of P_{700} photooxidation can be determined, at least partly, by changes in the redox state of the electron transport chain during dark adaptation of leaves: the plastoquinone pool is oxidized under aerobic conditions, while it remains largely reduced under anaerobic conditions [56-59]. Our fluorescence measurements also support this inference. Figure 4 shows representative fluorescence induction curves (fast stages) that were measured on dark-adapted Chinese hibiscus leaves incubated in air or in an atmosphere of argon. In the first case (10-min dark adaptation in air),

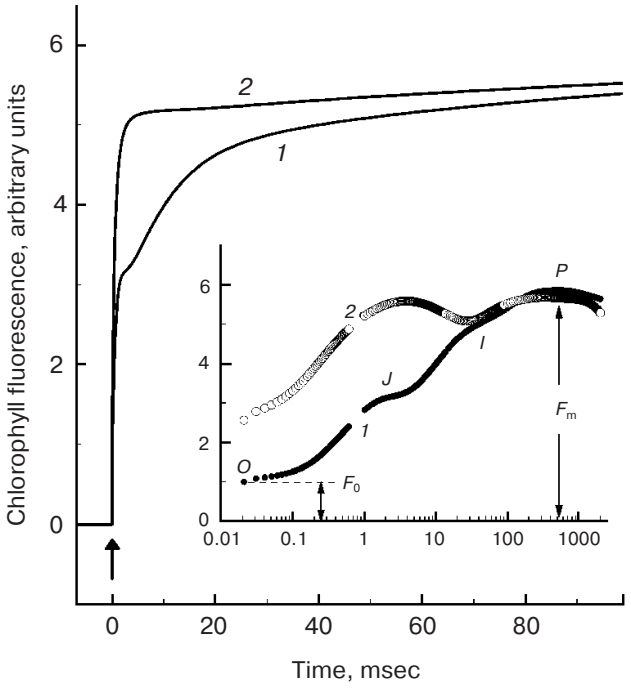

Fig. 4. Fast stages of the chlorophyll fluorescence induction curve in Chinese hibiscus leaves adapted to darkness for 10 min in air (*1*) and in argon atmosphere (*2*).

the fluorescence induction curve was multiphasic (*O-J-I-P* transitions), with fluorescence ratio $F_v/F_m = 0.83$, where F_v is "variable" fluorescence ($F_v = F_m - F_0$) and F_m is maximal fluorescence. This value is typical for dark-adapted leaves of C_3 plants [55, 57, 58]. Under aerobic conditions the fluorescence level increased during illumination almost sixfold compared to F_0 ($F_m/F_0 = 5.87$). Hence, in dark-adapted aerated leaves the major part of the plastoquinone pool was in the oxidized state.

In leaves incubated in the atmosphere of argon (or nitrogen), the initial fluorescence, F_0, was about 2.5 times higher than in aerobic conditions. The relative value of variable fluorescence (F_v/F_m) decreased to $F_v/F_m = 0.55$; furthermore, the fluorescence rise time was shortened by more than an order of magnitude. These data provide clear evidence that the pool of electron carriers between PS2 and PS1 becomes oxidized during dark adaptation of leaves under aerobic conditions, while the major part of this pool remains reduced during dark adaptation in an inert gas atmosphere. The most common explanation of this dependence is that plastoquinol (the main reservoir of electron carriers in the chain segment between the two photosystems) is oxidized in darkness by oxygen [56, 57, 59]. It is also possible that chloroplasts contain terminal oxidases that catalyze plastoquinol oxidation under aerobic conditions [14].

Effect of O_2 and CO_2 on non-photochemical quenching of chlorophyll fluorescence. Chlorophyll fluorescence measurements provide a means to quantify the efficiency of photochemical processes as well as heat dissipation of absorbed light energy in chloroplasts. PAM fluorometry allows researchers to separate the contributions of photochemical and non-photochemical fluorescence quenching [43-48]. The extent of non-photochemical quenching (NPQ), determined by heat losses in light-harvesting antenna of PS2, is known to increase upon acidification of the thylakoid inner space. Based on this knowledge, it is possible to use the NPQ parameter as an indicator of the thylakoid pH gradient (ΔpH).

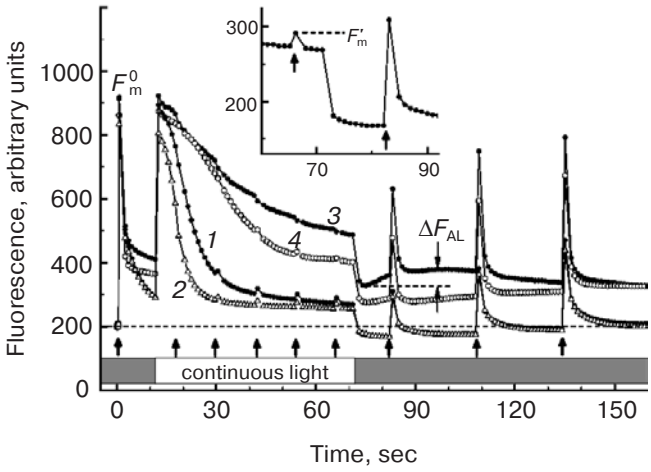

Fig. 5. Light-induced changes in chlorophyll fluorescence in Chinese hibiscus leaves as measured with the standard protocol for assaying non-photochemical fluorescence quenching using a PAM fluorometry (see text for details). Aerobic conditions ($[O_2] = 21\%$): *1*, *2*) first and second illumination, respectively; anaerobic conditions ($[O_2] < 0.5\%$): *3*, *4*) first and second illumination, respectively.

Figure 5 shows typical changes in chlorophyll fluorescence in Chinese hibiscus leaves as measured with conventional PAM fluorometry [45]. Arrows indicate the moments when saturation light pulses were applied either in darkness or on the background of continuous actinic light. The F_m^0 parameter designates the maximum fluorescence induced in a dark-adapted leaf by the first saturation pulse. After switching on continuous actinic light, fluorescence first increases rapidly and then diminishes slowly. Such non-monotonic time pattern, termed "slow fluorescence induction transients" has long been known and is well studied (see reviews [35, 43-49]). The extent of F'_m fluorescence, probed by short saturating light pulses on the background of continuous actinic light, also lowers during prolonged illumination. This lowering reflects the decrease in quantum yield of chlorophyll fluorescence caused by the enhancement of non-photochemical fluorescence quenching. The extent of non-photochemical quenching is quantified with an NPQ parameter [45]:

$$NPQ = (F_m^0 - F'_m)/F'_m. \quad (1)$$

Curves *1* and *2* in Fig. 5 were obtained during two successive illumination cycles of the same sample; the sample was dark-adapted for 10 min under aerobic conditions prior to each illumination. In analogy with kinetics of P_{700} photooxidation described above (Fig. 2), slow fluorescence transients also differed in response to the first (curve *1*) and the second (curve *2*) illumination. During the second illumination cycle, the fluorescence decline was conspicuously faster than in the first cycle (dark adaptation without pre-illumination). This observation might indicate that the transthylakoid ΔpH is generated faster in pre-illuminated than in dark-adapted leaves. The "memory" about pre-illumination is retained for at least 10 min during dark adaptation. The distinctive effects of the first and the second illumination cycles were also evident under anaerobic conditions (Fig. 5, curves *3* and *4*). Under anaerobic conditions, the fluorescence decline induced by continuous light proceeded markedly slower than under aerobic conditions (Fig. 5, curves *1* and *2*).

Another distinction between the samples incubated aerobically or anaerobically is that the fluorescence measured after switching off continuous light was substantially lower in leaves incubated under aerobic conditions (curves *1* and *2*) than in leaves placed in oxygen-free gas medium (curves *3* and *4*). In the latter case, the initial fluorescence decline after switching off the light was followed by a subsequent increase in fluorescence. The fluo-

rescence rise in darkness (ΔF_{AL} parameter in Fig. 5) is usually ascribed to the reduction of the plastoquinone pool [3, 60]. The fluorescence increase observed in darkness under anaerobic conditions is thought to originate because the rate of plastoquinone reduction by electron input from endogenous donors exceeds the rate of the oxidation of the pool. The supposed electron donors for plastoquinone reduction are reduced metabolites (e.g. NADPH) accumulated during illumination. The electron transport chain from NADPH to plastoquinone might comprise the chloroplast NAD(P)H dehydrogenase [60]. The other pathway for plastoquinone reduction is represented by a "short" cyclic electron transport chain comprising presumably a pgr-5 protein [3, 58]. The dark increase in fluorescence was manifested much weaker under aerobic conditions than under anaerobiosis (Fig. 5). A reasonable explanation is that plastoquinol is oxidized in darkness by atmospheric oxygen and that this process exceeds the relatively slow reduction of plastoquinone by electrons supplied from endogenous reductants. According to our estimates, the characteristic time of plastoquinone pool oxidation in air is $t_{1/2}$ ~ 2-3 min, which is consistent with previously reported data for Chinese hibiscus leaves [59].

Figure 6 shows effect of gas phase composition on photoinduced changes of the NPQ parameter. It is seen that illumination of a leaf placed in an atmosphere of nitrogen (curve *4*) induces a noticeably slower increase in NPQ compared to illumination under aerobic conditions (curve *1*). This indicates that the light-induced acidification of the thylakoid space is less pronounced in an oxygen-free environment than in normal air. The decrease in ΔpH could be related to retardation of electron flow between PS2 and PS1 when the acceptor side limitation arises in PS1 under shortage of oxygen. Under anaerobic conditions, some alternative pathways for electron efflux from PS1 (the Mehler reaction and photorespiration) are ineffective; this would lead to excessive accumulation of reduced acceptors on the PS1 acceptor side and, consequently, suppress linear electron flow and ΔpH generation.

It should be noted that the release of non-photochemical quenching upon oxygen depletion could be explained, in principle, not only by inhibition of the Mehler reaction, but also by the Warburg effect. The meaning of the latter phenomenon is that CO_2 fixation in the Calvin cycle of C_3 plants is stimulated by anaerobiosis owing to inhibition of photorespiration [35]. Obviously, the intensified operation of the Calvin cycle should promote ATP consumption, while the reduction of ATP content should result in faster turnover of ATP synthases and might lower the ΔpH. However, one should keep in mind that metabolic processes involved in photorespiration are also associated with ATP consumption, similarly to the Calvin cycle reactions [35]. The analysis of possible relations between the Warburg effect and the release of non-photochemical quenching would need special studies going beyond the scope of the present work.

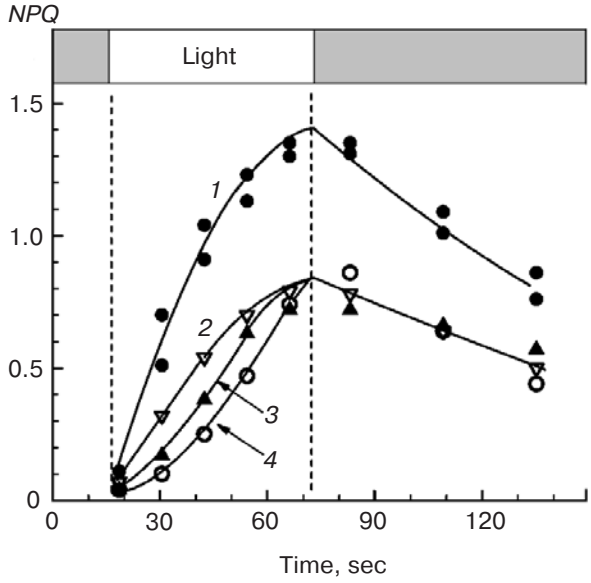

Fig. 6. Effect of atmospheric gas composition on non-photochemical quenching of chlorophyll fluorescence in a Chinese hibiscus leaf adapted to darkness for 10 min without pre-illumination. The leaf was adapted to darkness under the following conditions: *1*) atmospheric air; *2*) air with elevated CO_2 content (1%); *3*) nitrogen atmosphere with elevated CO_2 content (1%); *4*) nitrogen atmosphere.

It should be emphasized that the described effects of de-aeration cannot result exclusively from a possible depletion of endogenous CO_2 (terminal electron acceptor under physiological conditions), although the loss of CO_2 could occur during flushing the leaf with CO_2-free inert gas (N_2 or Ar). A reasonable assumption is that short-term (~10 min) flushing of the sample with inert gas effectively removes oxygen from the leaf but is insufficient for the depletion of CO_2 (and/or HCO_3^-) in the chloroplast stroma and for inhibition of the Calvin cycle. This is evident from observations of a significant decrease in NPQ even upon flushing the leaf by oxygen-free gas mixture enriched in CO_2 content. From the comparison of curves *2* (air + CO_2) and *3* (N_2 + CO_2) in Fig. 6, it is seen that oxygen depletion significantly released non-photochemical quenching even in the presence of excessive CO_2 content (~0.5-1%).

Remarkably, increase in CO_2 partial pressure (up to ~0.5-1%) in the aerobic atmosphere ($[O_2]$ = 21%) resulted in the release of NPQ rather than its increase (cf. curves *1* and *2* in Fig. 6). This observation is similar to the results obtained by Kramer and colleagues with *Nicotiana tabacum* leaves [61-63]. The release of non-photochemical quenching upon the increase in CO_2 content seems a paradoxical phenomenon at first sight. Indeed, one could expect that the increase in CO_2 partial pressure would stimulate noncyclic electron transport, thereby causing

stronger acidification of the thylakoid lumen and the respective increase in NPQ. However, the opposite effect was actually observed: the increase in CO_2 concentration resulted in a discernible decrease in NPQ (Fig. 6, curves *1* and *2*). This result can be explained by taking into account that stimulation of the Calvin cycle reactions at high CO_2 content not only accelerates electron transport on the PS1 acceptor side (this acceleration of electron flow would promote the increase in ΔpH) but may also lead to a decrease in ΔpH. Indeed, the acceleration of Calvin cycle reactions upon high CO_2 content stimulates ATP consumption and elevates ADP concentration. This would increase the ATP-synthase turnover and the proton flux through ATP-synthases with a concomitant decrease in ΔpH. Thus, the acceleration of Calvin cycle reactions at high CO_2 concentration may diminish the NPQ values.

In the above discussion of P_{700} redox transients, we mentioned a possibility that anaerobic conditions might stimulate cyclic electron flow around PS1, thereby increasing ΔpH. However, our experiments on leaves treated with DCMU, a PS2 inhibitor, have shown that non-photochemical quenching of chlorophyll fluorescence decreases slightly under anaerobic conditions in a marked contrast to its possible increase (data not shown). This observation is consistent with the kinetics of P_{700} redox transients (Fig. 3), corroborating the notion that anaerobic conditions do not accelerate cyclic electron flow.

Mathematical modeling of electron flows and proton transport. Here we analyze the above-described phenomena within the framework of a mathematical model developed previously [64-66]. The scheme of processes under consideration (Fig. 7) includes the main stages of electron and proton transport in thylakoids. According to this model, protons accumulate in the thylakoid lumen due to light-induced decomposition of water by PS2 and owing to plastoquinol (QH_2) oxidation by the cytochrome b_6f complex. The proton efflux from thylakoids occurs through the ATP-synthase (proton flux J_{ATP}) and through the passive leak unrelated to ATP synthesis (proton flux J_{pas}). Apart from ATP synthesis and $NADP^+$ reduction, consumption of ATP and NADPH in the Calvin cycle is taken into consideration. Branching of the electron flow on the acceptor side of PS1 is likely. The linear (non-cyclic) electron flow (PS1 → $NADP^+$) produces NADPH. The second pathway is a "short" cyclic electron flow that returns electrons from PS1 to the electron transport chain in the region between PS2 and PS1 (at the plastoquinone segment). In addition to this chain, there is another supposed cyclic route that returns electrons

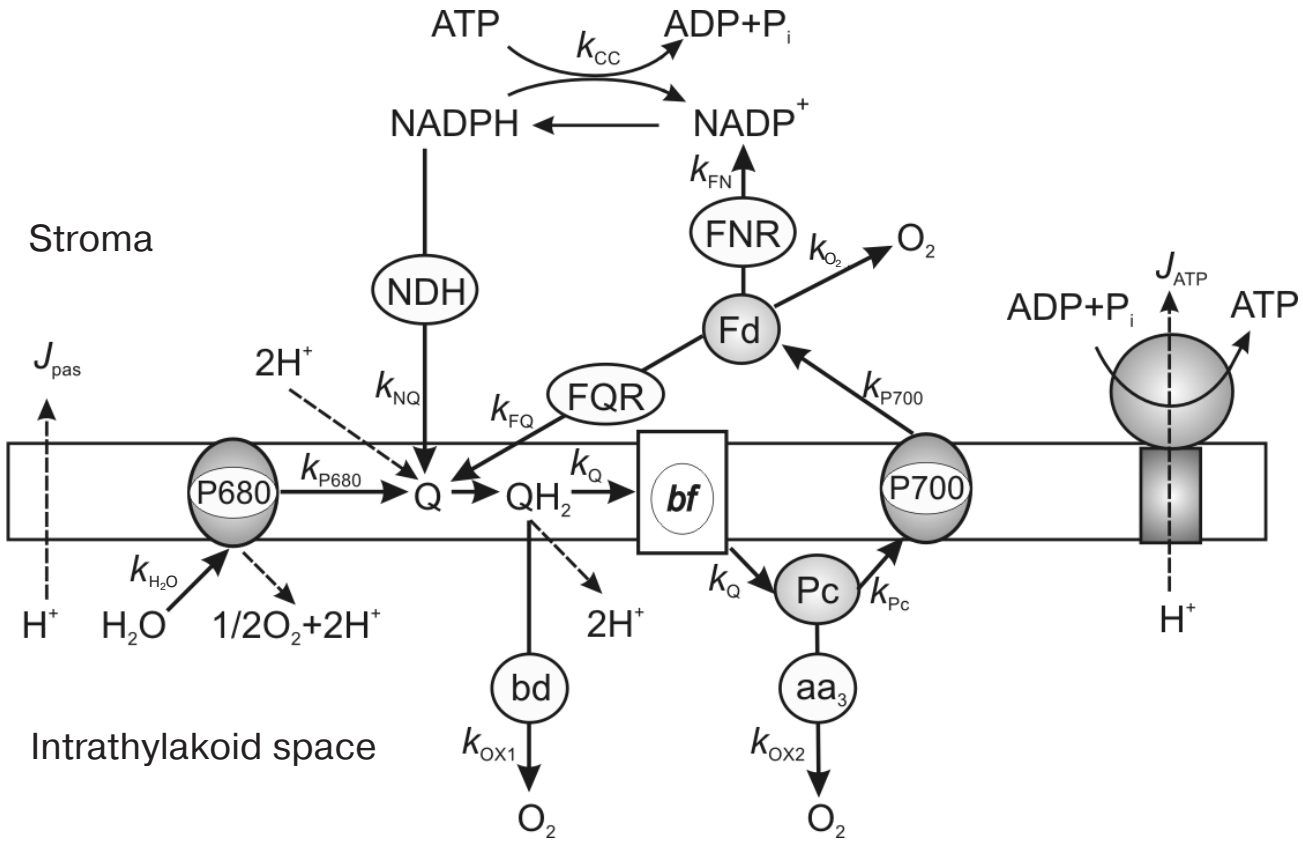

Fig. 7. Electron and proton transport processes considered in the model. Designations: NDH) NAD(P)H dehydrogenase; FQR) ferredoxin:quinone reductase; FNR) ferredoxin:NADP reductase; bd, aa_3) terminal oxidases of bd and aa_3 types.

from NADPH to the electron transport chain via NADPH dehydrogenase–plastoquinone reductase; this pathway is termed here a "long" cyclic electron flow. The third route for electron efflux from PS1 is the electron transport from ferredoxin to oxygen. In this work, electron flows from plastoquinone and plastocyanin to oxygen mediated by terminal oxidases were neglected, because these flows in chloroplasts are insignificant compared to the main electron flow from PS2 to PS1.

The model for describing electron-transport processes considers the following variables: $[P^+_{700}]$, concentration of oxidized P_{700} centers (primary electron donor in PS1); $[P^+_{680}]$, concentration of oxidized P_{680} centers (primary electron donor in PS2); $[Pc^+]$, concentration of the oxidized electron carriers acting as immediate donors for oxidized P_{700} centers (plastocyanin in plants and/or cytochrome c_6 in cyanobacteria); [Q], concentration of oxidized plastoquinone; $[Fd^+]$, concentration of oxidized ferredoxin; $[NADP^+]$, concentration of oxidized terminal acceptor in PS1 ($NADP^+$); $[O_2]$, oxygen concentration.

Differential equations describing the kinetics of redox transitions for electron carriers, pH changes in the thylakoid lumen (pH_i variable), as well as ATP synthesis and consumption processes ([ATP] variable) were considered in detail elsewhere [64-66]. The rate constants for key stages of electron flow and proton transport were determined by fitting respective experimental and simulated kinetic curves [64-68]. The stage of plastoquinol oxidation controlled by intra-thylakoid pH is a limiting step in the electron transport between PS2 and PS1. Effective rate constants for plastoquinol oxidation by the b_6f complex (k_Q), for electron transfer to plastocyanin, and for plastocyanin oxidation by oxidized P^+_{700} centers (k_{Pc}) were derived by comparing calculated and experimental plots for the rates of P^+_{700} dark reduction as a function of pH. Effective rate constants for the transmembrane proton transport coupled with ATP synthesis and for passive leak across the thylakoid membrane were determined from the comparison of calculated and experimental dependences of proton uptake on external pH (see [67, 68] for details).

The rate of electron efflux from PS1 to oxygen was calculated from the formula $J_{P_{700}} = k_{O_2}([Fd]_0 - [Fd^+])[O_2]$, where $[Fd]_0$ is the total concentration of oxidized and reduced ferredoxin forms. The effective rate constants for electron outflow to oxygen (k_{O_2}) was determined from comparison of experimental and theoretical dependences of steady-state P^+_{700} concentration on oxygen content in the ambient atmosphere. Figure 8a displays theoretical curves calculated for three values of $[Fd]_0/[P_{700}]_0$ parameter characterizing the relative size of ferredoxin pool molecules, where $[P_{700}]_0$ designates the total concentration of oxidized and reduced P_{700} forms. This figure also contains experimental data obtained on Chinese hibiscus leaves, as well as similar data obtained by Heber et al. on spinach leaves and presented in Fig. 5 of their publication [51]. It is worth noting that light intensities in experiments of Heber et al. [51] and in our experiments were quite similar. Data presented in Fig. 8a for Chinese hibiscus leaves were obtained under normal (~0.035%) and elevated CO_2 content (~0.5-1%) in the gas stream around the sample. Data for spinach leaves correspond to CO_2 concentration near the compensation point (0.0035%).

It is seen in Fig. 8 that the stationary P^+_{700} concentration diminishes with the decrease in $[O_2]$. Twofold decrease in $[P^+_{700}]$ was observed at oxygen concentrations ~2.5% in experiments with Chinese hibiscus leaves and ~5% in the case of spinach leaves. The difference between concentration dependences for Chinese hibiscus and spinach leaves could result from various causes. One pos-

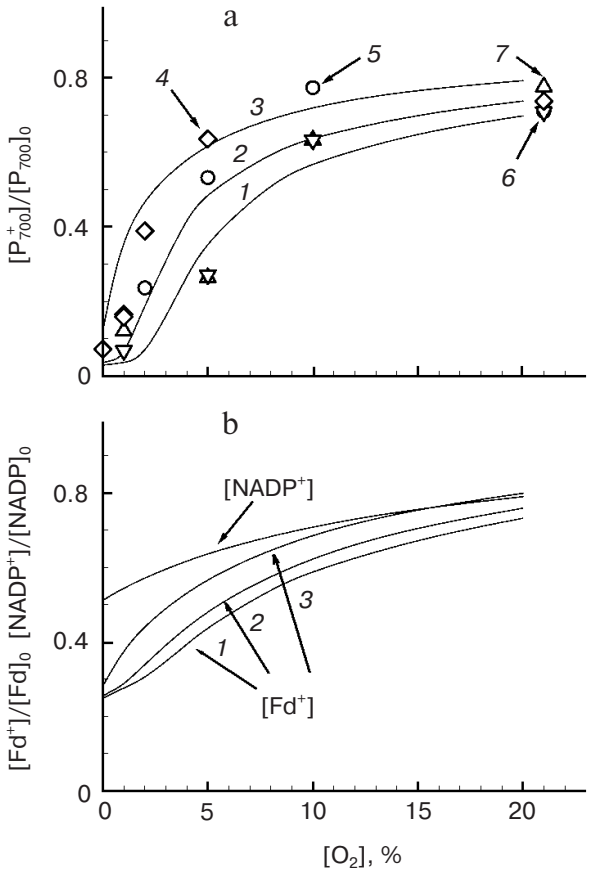

Fig. 8. Dependences of steady-state concentrations of P^+_{700} (a) and Fd^+ $NADP^+$ (b) on oxygen concentration. *1*, *2*, *3*) Theoretical curves calculated at $[Fd]_0/[P_{700}]_0$ parameter values of 4.5, 5, and 6, respectively. Other model parameters were $[NADP]_0/[P_{700}]_0$ = 10 and $[AdN]_0/[P_{700}]_0$ = 200, where $[NADP]_0$ is total concentration of oxidized and reduced NADP forms and $[AdN]_0$ is total concentration of ADP and ATP. Data points *4* and *5* represent experimentally measured values for Chinese hibiscus leaves at $[CO_2]$ = 0.035% (*4*) and $[CO_2]$ = 0.5-1% (*5*); data points *6* and *7* represent experimentally measured values with spinach leaves [51] at light intensities of 300 and 600 W/m^2.

sible reason is that the amounts of electron carriers in PS1 are different in these plant species. Figure 8a shows theoretical curves calculated with model parameters k_{O_2} = 8000 ($sec^{-1} \cdot M^{-1}$) and $[NADP]_0/[P_{700}]_0 = 10$ for three values of ferredoxin pool capacity, $[Fd]_0/[P_{700}]_0 = 4.5$, 5, and 6. It is seen that even slight variation of the ferredoxin pool size had a substantial effect on the shape of concentration dependences. The increase in the number of ferredoxin molecules was found to elevate the steady-state concentration of P^+_{700}. For Chinese hibiscus leaves, all experimental points fell into the region between two theoretical curves obtained for $[Fd]_0/[P_{700}]_0 = 5$ and 6. The data points for spinach leaves fell closer to the theoretical curve obtained at $[Fd]_0/[P_{700}]_0 = 4.5$. Thus, for adopted rate constant values characterizing ferredoxin oxidation by oxygen, the theoretical curves are in a reasonably good agreement with experimental data. The calculations showed that, under aerobic conditions (20% O_2), the electron flow to oxygen constitutes ~40% of the total electron flux passing through PS1. These estimates are consistent with available evidence [23-25] that the potential contribution of the "water–water" cycle is rather high. According to Makino et al. [24], the "water–water" cycle may contribute as much as 50% to the total electron flux through PS1 under normal conditions; these estimates are considerably higher than those of other authors [12-14].

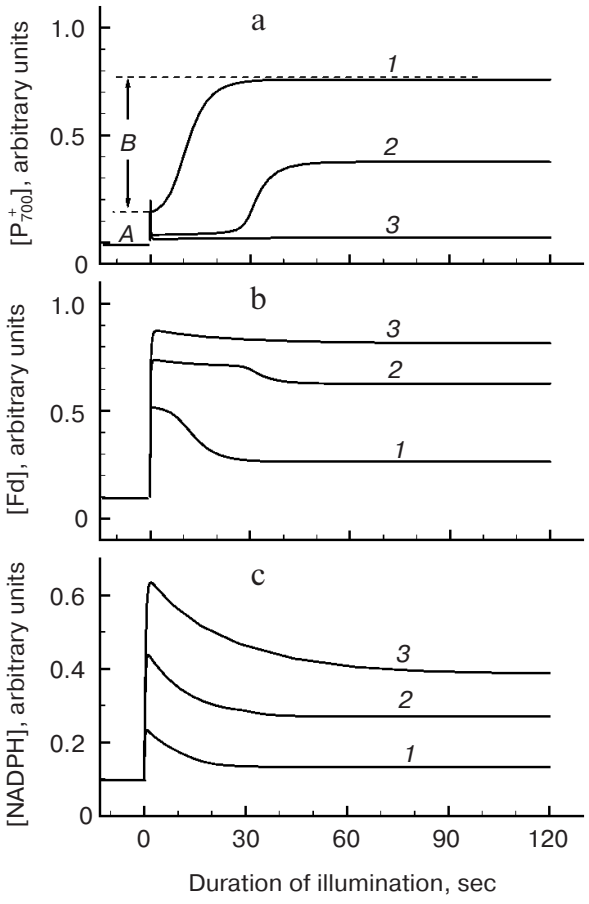

Fig. 9. Calculated kinetics of light-induced concentration changes for the following electron transport carriers: a) P^+_{700}; b) reduced ferredoxin; c) NADPH. Curves: *1*) 20% O_2 (atmospheric concentration); *2*) 5% O_2; *3*) 0.5% O_2. Parameter values were as follows: $[Fd]_0/[P_{700}]_0 = 5$, $[NADP]_0/[P_{700}]_0 = 10$, and $[AdN]_0/[P_{700}]_0 = 200$. The initial conditions for dark-adapted state were taken as follows: all P_{700} molecules are reduced, 90% of ferredoxin molecules and 90% NADP are in the oxidized state. Prior to illumination, the plastoquinone pool was 95% oxidized at $[O_2] = 20$ and 5%, and it was 5% oxidized at $[O_2] = 0.5\%$.

Figure 9 shows theoretical curves describing temporal pattern for relative concentrations of P^+_{700} (a), oxidized ferredoxin (b), and NADPH (c) at three oxygen concentration, namely, 20, 5.0, and 0.5%. The kinetic curves of $[P^+_{700}]$ changes in Fig. 9a are clearly multiphasic. During simulation of "aerobic" conditions, when electron efflux from PS1 to oxygen is taken into consideration, the initial jump in $[P^+_{700}]$ (stage *A*) was followed by $[P^+_{700}]$ decline; the secondary rise of $[P^+_{700}]$ toward the steady state (stage *B*) appeared after a lag phase. The third stage of P_{700} photooxidation, observed in experiments under aerobic conditions (Fig. 2), was not evident in calculated curves because the current model did not account for light-induced activation of Calvin cycle reactions [69]. When oxygen concentration was reduced to 5%, the lag phase became longer, while the steady-state concentration of P^+_{700} was lowered. Further strong reduction in electron flow to oxygen (at 0.5% O_2) strongly diminished the steady-state P^+_{700} concentration consistent with experimental data (Fig. 3). It should be noted that the shape of kinetic curves was not *a priori* defined in our model of electron and proton transport. As stated above, only effective constants for elementary steps of electron and proton transfer were optimized based on well-established experimental data.

Temporal changes of ferredoxin and NADPH were found to follow non-monotonic kinetic curves (Figs. 9b and 9c, respectively). The model predicts that switching on the light under aerobic conditions induces fast initial reduction of oxidized ferredoxin and $NADP^+$ molecules with the subsequent slow oxidation of both electron carriers. The steady-state concentrations of the reduced acceptors ([Fd] and [NADPH]) were comparatively high at low oxygen concentrations and diminished under oxygen excess conditions. By comparing the calculated curves of $[P^+_{700}]$ with the respective curves for [Fd] and [NADPH], we found that the lag phase duration in the kinetics of P_{700} photooxidation correlates with the reduction degree of ferredoxin and NADPH pools. It is seen that prolongation of the lag phase and decline in the stationary $[P^+_{700}]$ upon anaerobiosis corresponded to elevation in steady-state concentrations of [Fd] and [NADPH]. Thus, the results of our calculations are in a good agreement with the observed kinetic patterns of P_{700} photooxidation. These results are also consistent with the

assumption that "over-reduction" of the PS1 acceptor side is among causes opposing P_{700} photooxidation under hindrance of electron outflow from PS1 to oxygen.

Another factor affecting the kinetics of P_{700} photooxidation is the photoinduced acidification of the intra-thylakoid space. A decrease in pH_i is known to decelerate plastoquinol oxidation by the b_6f complex, which impedes the electron influx to P^+_{700} [37-42]. Figure 10 shows the kinetics of ATP concentration (a), the pH difference ($\Delta pH = pH_0 - pH_i$) (b), and electron flow from plastocyanin to P^+_{700} (c), as calculated for three oxygen concentrations. Electron flow toward P^+_{700} ($J_{P_{700}}$ variable) was calculated from the formula $J_{P_{700}} = k_{Pc}[Pc][P^+_{700}]$, where [Pc] is concentration of reduced plastocyanin and $k_{Pc} = 10^3$ ($[P_{700}]_0^{-1}$) sec^{-1} is the effective rate constant for electron transfer from Pc to P^+_{700}, determined in a previous study [67]. From comparison of Figs. 9a and 10 one can notice that the phase of comparatively slow photooxidation of P_{700} (phase *B*) is correlated with ΔpH increase (Fig. 10b) that reflects the transition of chloroplasts from metabolic state 3 to state 4 (depletion of ADP pool, Fig. 10a). After depletion of the ADP pool, the turnover rate for ATP-synthase complexes becomes slower; therefore, a stronger acidification of the intra-thylakoid space takes place. Consequently, plastoquinol oxidation by the b_6f complex becomes hindered, which is accompanied by deceleration of electron flow to PS1 (Fig. 10c) and by increase in P^+_{700} content (Fig. 9a).

Our calculations showed that the transition from aerobic to anaerobic conditions diminishes the transmembrane pH difference (Fig. 10b) and decelerates the ATP accumulation (Fig. 10a). These results nicely agree with our experimental data, suggesting that inhibition of electron outflow from PS1 to oxygen is accompanied by decrease in ΔpH, as deduced from the release of non-photochemical quenching under anaerobic conditions (Fig. 6). It appears that a comparatively small decrease in pH_i does not impose strong restrictions on electron transport between PS2 and PS1; therefore, the steady-state electron flow toward P^+_{700} is faster under anaerobic conditions than in aerobic conditions. This inference is clearly supported by our calculations (Fig. 10c). It is seen that the influence of oxygen on the flux $J_{P_{700}}$ is especially effective within 20-30 sec from the onset of illumination. Under aerobic conditions, the rate of electron supply to P^+_{700} immediately after switching on the light is noticeably higher than under low oxygen concentration. Further on, the rate of electron flow toward P^+_{700} decreases under aerobic conditions, in parallel with acidification of the intra-thylakoid space. At reduced oxygen content (5%) and under oxygen deficiency (0.5%), the calculated kinetic curves are more complex. It is remarkable that the sustained electron flow rate toward P^+_{700} is lower under aerobic conditions (20% O_2) compared to anaerobic conditions. Apparently, this effect reflects a stronger inhibition of electron transport at the state of plastoquinone oxidation, caused by stronger decrease in thylakoid pH under aerobic conditions (Fig. 10b).

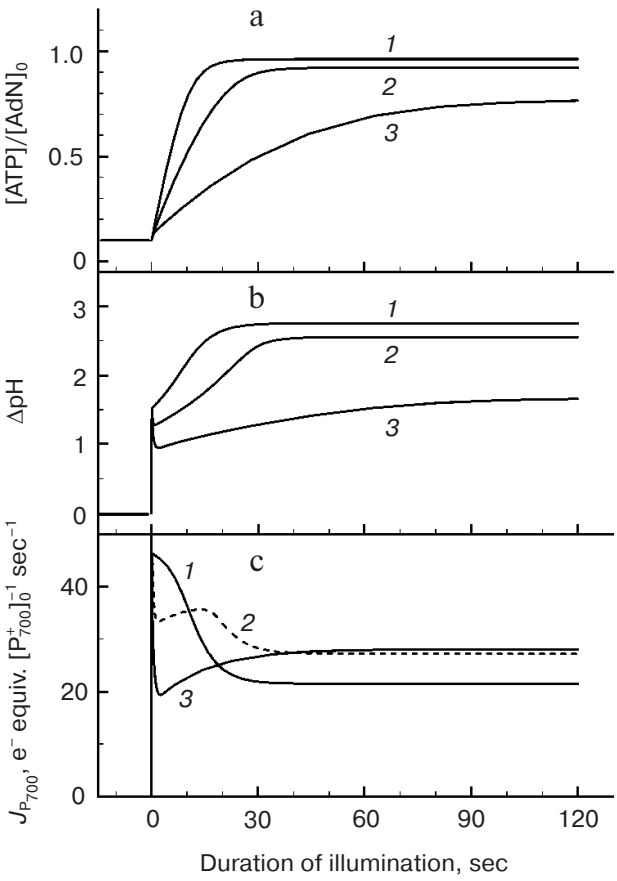

Fig. 10. Effect of oxygen content on calculated kinetics of light-induced changes in: a) ATP content; b) ΔpH; c) electron flow J_{P700}. Curves: *1*) 20% O_2 (atmospheric oxygen content); *2*) 5%; *3*) 0.5%.

Thus, the calculation results are fully consistent with experimental data and support the notion that electron efflux from PS1 to oxygen has a substantial influence on the kinetics of electron transport and ΔpH generation in chloroplasts. The increase in steady-state P^+_{700} concentration in the presence of oxygen, deduced from our calculations, can be explained as follows. On one hand, the electron efflux to oxygen prevents the excessive accumulation of reduced carriers on the acceptor side of PS1 and, on the other hand, it facilitates the suppression of electron flow toward P^+_{700} owing to stronger acidification of the intra-thylakoid space. The light-dependent electron flow to oxygen in the chloroplast photosynthetic electron transport chain eventually produces H_2O_2 molecules, which might act as a signal indicating the redox state of the plastoquinone pool [70].

Our kinetic study of light-induced EPR I signals attributed to oxidized P^+_{700} centers in leaves of *H. rosasinensis* shows that oxygen content in the ambient atmos-

phere has a conspicuous influence on photosynthetic electron transport. The sustained concentration of P^+_{700} centers oxidized during continuous actinic illumination is substantially lower in the oxygen-free environment than under aerobic conditions. A similar result was obtained with leaves of *V. faba*. The decrease in $[P^+_{700}]$ under anaerobic conditions can be caused by over-reduction of PS1 acceptor side upon blockade of the oxygen-dependent pathway for electron outflow from PS1, as well as by the release of photosynthetic control owing to weaker acidification of the thylakoid lumen. The latter inference is supported by the observed release of non-photochemical quenching of chlorophyll fluorescence, indicative of the thylakoid ΔpH. The comparison of experimental data with the results of numerical simulation of electron transport allowed us to estimate the fractional electron flux diverted from PS1 to oxygen. According to our estimates, this flux can be as large as 40% of the total electron flow passing through PS1. It should be noted that anaerobiosis does not stimulate cyclic electron transport around PS1, even though this possibility seemed likely in view of redistribution of electron flows on the acceptor side of PS1. This conclusion is evidenced by observations that anaerobic conditions neither accelerated dark reduction of P^+_{700} in leaves treated with DCMU nor stimulated non-photochemical quenching of chlorophyll fluorescence in the presence of this PS2 inhibitor.

We are grateful to B. N. Ivanov and the reviewer for constructive criticism and valuable comments.

This work was supported by the Russian Foundation for Basic Research, project No. 06-04-48620.

REFERENCES

1. Bendall, D. S., and Manasse, R. S. (1995) *Biochim. Biophys. Acta*, **1229**, 23-38.
2. Allen, J. (2003) *Trends Plant Sci.*, **8**, 15-19.
3. Munekage, Y., Hashimoto, M., Miyake, C., Tomizawa, K.-I., Endo, T., Tasaka, M., and Shikanai, T. (2004) *Nature*, **429**, 579-582.
4. Joet, T., Cournac, L., Peltier, G., and Havaux, M. (2002) *Plant Physiol.*, **128**, 760-769.
5. Joliot, P., and Joliot, A. (2002) *Proc. Natl. Acad. Sci. USA*, **99**, 10209-10214.
6. Joliot, P., and Joliot, A. (2005) *Proc. Natl. Acad. Sci. USA*, **102**, 4913-4918.
7. Johnson, G. N. (2005) *J. Exp. Bot.*, **56**, 407-416.
8. Breyton, C., Nandha, B., Johnson, G., Joliot, P., and Finazzi, G. (2006) *Biochemistry* **45**, 13465-13475.
9. Golding, A. J., and Johnson, G. N. (2003) *Planta*, **218**, 107-114.
10. Talts, E., Oja, V., Ramma, H., Rasulov, B., Anijalg, A., and Laisk, A. (2007) *Photosynth. Res.*, **94**, 109-120.
11. Mehler, A. H. (1951) *Arch. Biochem. Biophys.*, **33**, 65-77.
12. Asada, K. (1999) *Annu. Rev. Plant Physiol. Plant Mol. Biol.*, **50**, 601-639.
13. Heber, U. (2002) *Photosynth. Res.*, **73**, 223-231.
14. Peltier, G., and Cournac, L. (2002) *Annu. Rev. Plant Biol.*, **53**, 523-550.
15. Badger, M. R., von Caemmerer, S., Ruuska, S., and Nakano, H. (2000) *Philos. Trans. R. Soc. Lond. B*, **355**, 1433-1446.
16. Backhausen, J. E., Kitzmann, C., Horton, P., and Scheibe, R. (2000) *Photosynth. Res.*, **64**, 1-13.
17. Foyer, C. H., and Noctor, G. (2000) *J. Exp. Bot.*, **51**, 15-19.
18. Allen, J., and Fosberg, J. (2001) *Trends Plant Sci.*, **6**, 317-326.
19. Kramer, D. M., Sacksteder, C. A., and Cruz, J. A. (2003) *Trends Plant Sci.*, **8**, 27-32.
20. Kramer, D. M., Avenson, T. J., and Edwards, G. E. (2004) *Trends Plant Sci.*, **9**, 349-357.
21. Ruuska, S. A., Badger, M. R., Andrews, T. J., and von Caemmerer, S. (2000) *J. Exp. Bot.*, **51**, 357-368.
22. Sage, F. R., Cen, Y.-P., and Li, M. (2002) *Photosynth. Res.*, **71**, 241-250.
23. Miyake, C., and Yokota, A. (2000) *Plant Cell. Physiol.*, **41**, 335-343.
24. Makino, A., Miyake, C., and Yokota, A. (2002) *Plant Cell. Physiol.*, **43**, 1017-1026.
25. Osmond, C. B., and Grace, S. C. (1995) *J. Exp. Bot.*, **46**, 1351-1362.
26. Ziem-Hanck, U., and Heber, U. (1980) *Biochim. Biophys. Acta*, **591**, 266-274.
27. Ivanov, B., Kobayashi, Y., and Heber, U. (1998) *Photosynth. Res.*, **57**, 61-70.
28. Cornic, G., and Briantais, J.-M. (1991) *Planta*, **183**, 178-184.
29. Vishnyakova, E. A., Trubitsin, B. V., and Tikhonov, A. N. (2000) *Biofizika*, **45**, 899-904.
30. Chow, W. S., and Hope, A. B. (2002) *Photosynth. Res.*, **81**, 77-89.
31. Joliot, P., and Joliot, A. (2006) *Biochim. Biophys. Acta*, **1757**, 362-368.
32. Maxwell, P. C., and Biggins, J. (1977) *Biochim. Biophys. Acta*, **459**, 442-450.
33. Trubitsin, B. V., Mamedov, M. D., Vitukhnovskaya, L. A., Semenov, A. Yu., and Tikhonov, A. N. (2003) *FEBS Lett.*, **544**, 15-20.
34. Trubitsin, B. V., Ptushenko, V. V., Koksharova, O. A., Mamedov, M. D., Vitukhnovskaya, L. A., Grigor'ev, I. A., Semenov, A. Yu., and Tikhonov, A. N. (2005) *Biochim. Biophys. Acta*, **1708**, 238-249.
35. Edwards, G. E., and Walker, D. A. (1983) *C3, C4: Mechanisms and Cellular and Environmental Regulation of Photosynthesis*, Blackwell Scientific, Oxford.
36. Allen, J. F. (1992) *Biochim. Biophys. Acta*, **1098**, 275-335.
37. Rumberg, B., and Siggel, U. (1969) *Naturwissenschaften*, **56**, 130-132.
38. Stiehl, H. H., and Witt, H. T. (1969) *Z. Naturforsch. Teil B*, **24**, 1588-1598.
39. Tikhonov, A. N., Khomutov, G. B., Ruuge, E. K., and Blumenfeld, L. A. (1981) *Biochim. Biophys. Acta*, **637**, 321-333.
40. Haehnel, W. (1984) *Annu. Rev. Plant Physiol. Plant Mol. Biol.*, **35**, 659-693.
41. Blumenfeld, L. A., and Tikhonov, A. N. (1994) *Biophysical Thermodynamics of Intracellular Processes. Molecular Machines of the Living Cell*, Spinger Verlag, N. Y.
42. Kramer, D. M., Sacksteder, C. A., and Cruz, J. A. (1999) *Photosynth. Res.*, **60**, 151-163.

43. Horton, P., Ruban, A. V., and Walters, R. G. (1996) *Annu. Rev. Plant Physiol. Plant Mol. Biol.*, **47**, 655-684.
44. Niyogi, K. (1999) *Ann. Rev. Plant Physiol. Plant Mol. Biol.*, **50**, 333-359.
45. Maxwell, K., and Johnson, G. N. (2000) *J. Exp. Bot.*, **51**, 659-668.
46. Mueller, P., Li, X. P., and Niyogi, K. K. (2001) *Plant Physiol.*, **125**, 1558-1566.
47. Niyogi, K. K., Li, X. P., Rosenberg, V., and Jung, H. S. (2004) *J. Exp. Bot.*, **56**, 375-382.
48. Karapetyan, N. V. (2007) *Biochemistry* (Moscow), **72**, 1127-1135.
49. Rabinowitch, E. (1956) *Photosynthesis*, Vol. 3, Interscience Publishers, New York.
50. Webber, A. N., and Lubitz, W. (2001) *Biochim. Biophys. Acta*, **1507**, 61-79.
51. Heber, U., Neimanis, S., Siebke, K., Schonknecht, G., and Katona, E. (1992) *Photosynth. Res.*, **34**, 443-447.
52. Savitsky, A., Trubitsin, B. V., Mobius, K., Semenov, A. Yu., and Tikhonov, A. N. (2007) *Appl. Magn. Reson.*, **31**, 221-236.
53. Tagawa, K., Tsujimoto, H. Y., and Arnon, D. (1963) *Nature*, **199**, 1247-1252.
54. Kobayashi, Y., and Heber, U. (1994) *Photosynth. Res.*, **41**, 419-428.
55. Lazar, D. (1999) *Biochim. Biophys. Acta*, **1412**, 1-28.
56. Khorobrykh, S. A., and Ivanov, B. N. (2002) *Photosynth. Res.*, **71**, 209-219.
57. Toth, S. Z., Schansker, G., and Strasser, R. J. (2007) *Photosynth. Res.*, **93**, 193-203.
58. Nandha, B., Finazzi, G., Joliot, P., Hald, S., and Johnson, G. N. (2007) *Biochim. Biophys. Acta*, **1767**, 1252-1259.
59. Karavaev, V. K., and Kukushkin, A. K. (1975) *Biofizika*, **20**, 88-92.
60. Burrows, P. A., Sazanov, L. F., Svab, Z., Maliga, P., and Nixon, P. J. (1998) *EMBO J.*, **17**, 868-876.
61. Kanazawa, A., and Kramer, D. M. (2002) *Proc. Natl. Acad. Sci. USA*, **99**, 12789-12794.
62. Avenson, T. J., Cruz, J. A., and Kramer, D. M. (2004) *Proc. Natl. Acad. Sci. USA*, **101**, 5530-5535.
63. Takizawa, K., Cruz, J. A., Kanazawa, A., and Kramer, D. M. (2007) *Biochim. Biophys. Acta*, **1767**, 1233-1244.
64. Vershubskii, A. V., Priklonskii, V. I., and Tikhonov, A. N. (2004) *Biochemistry* (Moscow), **69**, 1016-1024.
65. Vershubskii, A. V., Priklonskii, V. I., and Tikhonov, A. N. (2006) *Fiz. Khim.*, **80**, 552-559.
66. Vershubskii, A. V., Priklonskii, V. I., and Tikhonov, A. N. (2007) *Khim. Fiz.*, **26**, 54-64.
67. Dubinskii, A. Yu., and Tikhonov, A. N. (1994) *Biofizika*, **39**, 652-665.
68. Dubinskii, A. Yu., and Tikhonov, A. N. (1995) *Biofizika*, **40**, 365-371.
69. Frolov, A. E., and Tikhonov, A. N. (2007) *Biofizika*, **52**, 656-666.
70. Ivanov, B. N. (2008) *Biochemistry* (Moscow), **73**, 112-117.